Shunt screening, size effects and I/V analysis in thin-film photovoltaics

V. G. Karpov,[a] G. Rich, A. V. Subashiev,[b] and G. Dorer
First Solar, LLC, 12900 Eckel Junction Road, Perrysburg, Ohio 43551

(Received 2 January 2001; accepted for publication 5 February 2001)

We present an analytical model that quantitatively describes the physics behind shunting in thin film photovoltaics and predicts size-dependent effects in the I/V characteristics of solar cells. The model consists of an array of microdiodes and a shunt in parallel between the two electrodes, one of which mimics the transparent conductive oxide and has a finite resistance. We introduce the concept of the screening length L, over which the shunt affects the system electric potential. The nature of this screening is that the system generates currents in response to the point perturbation caused by the shunt. L is expressed explicitly in the terms of the system parameters. We find the spatial distribution of the electric potential in the system and its I/V characteristics. The measured I/V characteristics depend on the relationship between the cell size l and L, being markedly different for the cases of small ($l \ll L$) and large ($l \gg L$) cells. We introduce a new regime of the large photovoltaic cell where all the characteristics are calculated analytically. Our model is verified both numerically and experimentally: good agreement is obtained. © *2001 American Institute of Physics.* [DOI: 10.1063/1.1359158]

I. INTRODUCTION

It has been long recognized that shunts are detrimental to thin-film photovoltaic (PV) cells. While it is intuitively clear that a shunt robs the current from a finite surrounding area, understanding of shunting has never been developed to the extent that would allow one to calculate that area depending on the shunt resistance, material parameters, and light intensity. Deriving and verifying the latter dependencies is one of the main goals of this article.

From the general perspective, the aforementioned question raises the problem of a point perturbation in a PV cell and how that perturbation is screened in the cell. This problem has one other important implication. Suppose we apply a voltage (V) across the cell by attaching two point contacts to its planar electrodes and measure the integral current (I) in the cell. At each point, the current density depends on local voltage across the cell. As a result, the electric potential nonuniformity caused by a point contact is screened by the currents and because of that screening, only a finite fraction of the cell will respond to the bias. Therefore, the measured I/V characteristics of the cell will depend on the relationship between the cell size l and the screening length L, being markedly different for the cases of small ($l \ll L$) and large ($l \gg L$) cells. If L is voltage dependent (as follows) the situation becomes even more complicated and the standard interpretation of the PV cell I/V characteristics needs to be revised.

This problem of I/V analysis was posed in the terms of distributed series resistance in solar cells.[1–4] In Ref. 1, a transcendental equation was derived aimed at describing I/V characteristics of one-dimensional p-n junctions. However, neither the concept of screening, nor the electric potential distribution analyses were advanced there. Subsequent publications[2–4] utilized the same physics as in Ref. 1 to develop numerical approaches and verify calculated I/V curves. This article adds more analytical results to the field of thin-film PV cell I/V characteristics. In particular, it introduces the limiting large PV cell case and criterion, for which the I/V characteristics are obtained explicitly in a closed form. More importantly, our consideration provides one with a simple intuitive approach applicable to both one- and two-dimensional device geometry and describes cell behavior in the whole range of light intensities and biases. This approach also offers a natural scope to describe shunt (and other macroscopic defect) effects on thin-film PVs.

In what follows, we concentrate mostly on the simplest conceivable model, that is a one-dimensional cell that adequately exhibits screening and size-dependent phenomena and at the same time enables one to derive closed analytical solutions. Side by side with that we give the related results for the case of two-dimensional (''dot'') cell. Numerical calculations and experiments are shown to verify our analytical results.

This article is organized as follows. In Sec. II, we give a qualitative consideration of screening phenomena and electric potential distribution in the cell. In Sec. III a rigorous mathematical approach is developed for the case of one-dimensional geometry, including exact results for the regimes of large and small cells. Sec. IV contains modifications of the latter results to the dot cell geometry. Sec. V is devoted to verification of our predictions. Sec. VI contains general discussion and conclusions.

II. QUALITATIVE ANALYSIS

Our prototype equivalent circuit and its one-dimensional implementation are shown in Fig. 1. It consists of a multi-

[a]Electronic mail: vkarpov@firstsolar.com
[b]Also at: State Technical University, St. Petersburg, 195251, Russia.

 © 2001 American Institute of Physics

Downloaded 17 Apr 2001 to 209.45.202.202. Redistribution subject to AIP copyright, see http://ojps.aip.org/japo/japcr.jsp

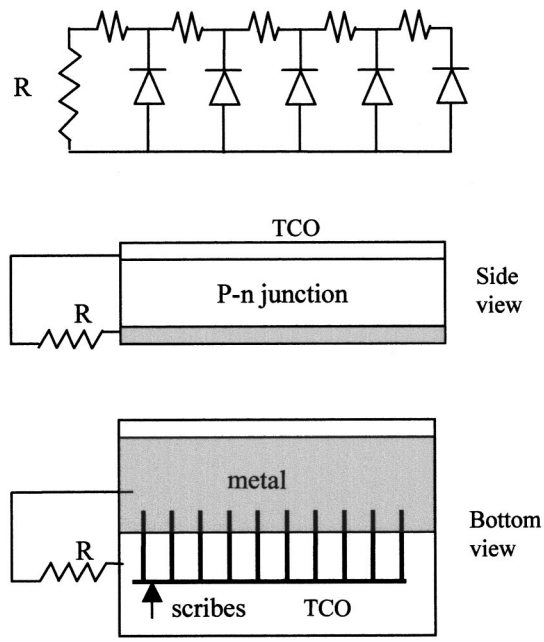

FIG. 1. The equivalent circuit and its one-dimensional implementation for a shunted PV cell.

tude of elemental PV cells in parallel with a resistor R that models a shunt. One of the electrodes in the circuit has a finite resistance ρ per length and mimics the transparent conductive oxide (TCO), typically used as a front contact. The second (metal) electrode has a negligibly small resistance.

A two-dimensional (dot cell) version of the same equivalent circuit is shown in Fig. 2. The dot-cell size is determined by the diameter of a metal-coated region. Again, resistor R models a shunt between the metal and TCO. In both cases, we assume a circuit where a voltage source V and ammeter in series with the resistor are used to measure the device I/V characteristics.

Each elemental diode in the model is described by the classical photodiode equation

$$j=j_0\left(\exp\left(\frac{q\varphi}{AkT}\right)-1\right)-j_L, \tag{1}$$

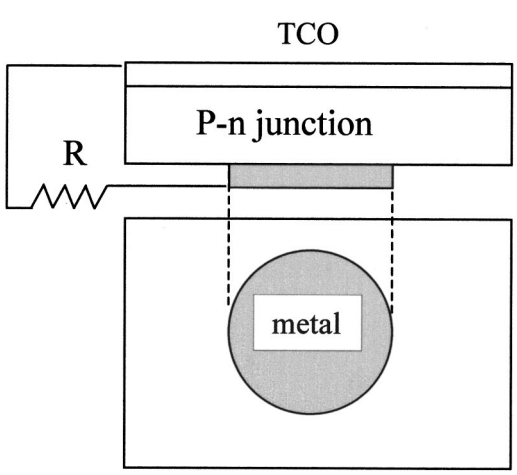

FIG. 2. Two-dimensional implementation of a shunted PV cell.

where j is the electric current in a diode, φ is electric potential, k is the Boltzmann's constant, q is the electron charge, A is the diode ideality factor, and j_0 and j_L stand for the thermal and photogenerated currents per length. These currents are related via the open circuit voltage V_{oc},

$$j_0\left(\exp\left(\frac{qV_{oc}}{AkT}\right)-1\right)=j_L. \tag{2}$$

For qualitative analysis, we start with a dead shunt in one-dimensional cell and neglect the thermal generation current j_0. Approximating the electric potential by linear coordinate dependence in the region of length L (Fig. 3), and noting that the current through the resistive electrode is supplied by the elemental cells in that region, gives

$$\frac{V_{oc}}{L\rho}=j_L L. \tag{3}$$

From that we find, the dead shunt screening length

$$L=L_{ds}\equiv\sqrt{\frac{V_{oc}}{j_L\rho}}. \tag{4}$$

One can say that the currents generated in response to the change in electric potential screen the shunt.

Along the same lines we write for a finite resistance shunt:

$$\frac{V_{oc}-V_R}{L\rho}=j_L L=\frac{V_R}{R},$$

where V_R is the potential drop across the shunt. This gives the screening length

$$L=L_{ds}\sqrt{1-\frac{V_R}{V_{oc}}},$$
$$\frac{V_R}{V_{oc}}=\frac{r}{2}(\sqrt{r^2+4}-r),\quad r\equiv\frac{R}{L_{ds}\rho}. \tag{5}$$

Next, consider the screening of an external bias. For the case of reverse or slightly forward biased cell, one can write [see Fig. 3(a)]

$$\frac{V_{oc}-V}{L\rho}=j_L L,$$

where the electric potential $V<V_{oc}$. As a result, the screening length becomes

$$L=\sqrt{\frac{V_{oc}-V}{j_L\rho}}. \tag{6}$$

For a significantly forward bias, $q(V-V_{oc})\gg kT$ the thermal current dominates the screening; therefore [see Fig. 3(b)]

$$\frac{V-V_{oc}}{\rho L}=j_0 L\exp\left(\frac{qV}{AkT}\right)\approx j_L L\exp\left[\frac{q(V-V_{oc})}{AkT}\right],$$

and

$$L=\sqrt{\frac{V-V_{oc}}{j_L\rho}}\exp\left[-\frac{q(V-V_{oc})}{2AkT}\right]. \tag{7}$$

Downloaded 17 Apr 2001 to 209.45.202.202. Redistribution subject to AIP copyright, see http://ojps.aip.org/japo/japcr.jsp

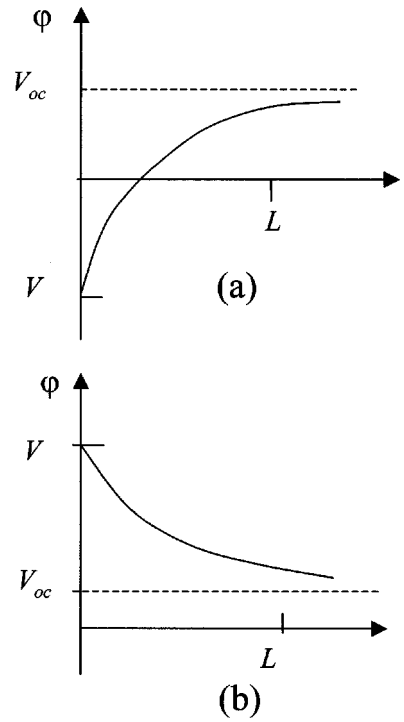

FIG. 3. The electric potential distributions in a semi-infinite one-dimensional PV cell under reverse (a) and forward (b) bias.

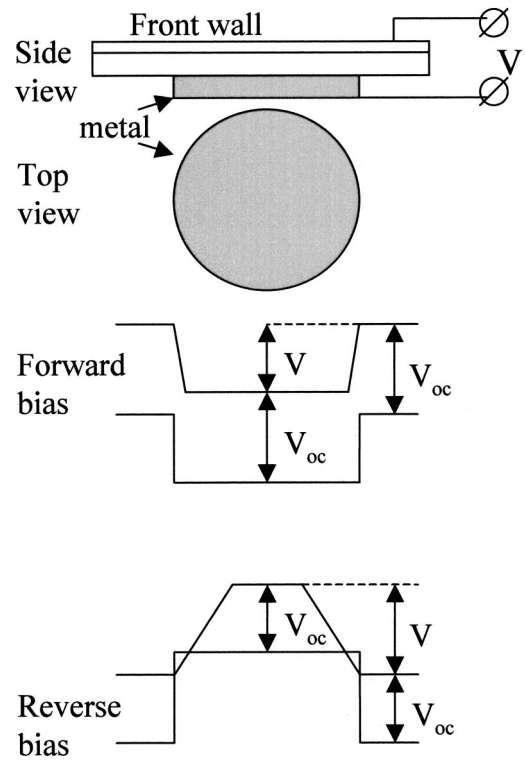

FIG. 4. Sketches of the electric potential distribution in a large dot cell in the cases of forward and reverse bias. Note that the electric potential is nonlinear in space and is approximated by straight lines.

We observe that the forward bias is screened over exponentially short distances. Exponentially strong currents forced through forward biased microdiodes are responsible for such screening.

In the same spirit, the I/V characteristics of the system are given by

$$I=\frac{\delta V}{R_{\mathrm{eff}}}, \quad R_{\mathrm{eff}}=\rho L, \tag{8}$$

where δV is the voltage drop across the system and the effective resistance R_{eff} is determined by the region of the screening length L where the current is collected.

For a reverse bias [$V<0$; see Fig. 3(a)] or not a very large forward bias ($V<V_{\mathrm{oc}}$) we get

$$\delta V=V_{\mathrm{oc}}-V, \quad I=-\sqrt{\frac{j_L(V_{\mathrm{oc}}-V)}{\rho}}. \tag{9}$$

For a significant forward bias, $q(V-V_{\mathrm{oc}})\gg kT$ [Fig. 3(b)] we obtain

$$\delta V=V-V_{\mathrm{oc}}, \quad I=\sqrt{\frac{(V-V_{\mathrm{oc}})j_L}{\rho}}\exp\left(\frac{q(V-V_{\mathrm{oc}})}{2AkT}\right). \tag{10}$$

For numerical estimate, consider a 1 cm wide strip cut off the typical PV cell where the resistive electrode sheet resistance is 10 Ω (and correspondingly, $\rho=10$ Ω/cm in these equations), $V_{\mathrm{oc}}=1$ V, and $j_L=20$ mA/cm. For these parameters we get from Eq. (4) $L_{\mathrm{ds}}=2.2$ cm. Hence, the dead shunt screening length is macroscopically large and can be measured directly (see the following).

The standard PV cell analyses tacitly imply the electric characteristics to be uniform across the resistive electrode, which in our terminology corresponds to the case of a small cell, $l\ll L$. Because L is comparable to the typical solar cell size l (~1 cm), both the regimes of small ($l\ll L$) and large ($l\gg L$) cells are possible in the course of I/V measurements. Furthermore, since L is voltage dependent, these regimes can show up in the complimentary regions of the same *I/V* curve. Specific examples will be given in Sec. V.

The aforementioned qualitative analysis can be extended to the two-dimensional case (Fig. 2). Taking into account that the longitudinal resistance of a sheet is almost independent of the sheet size and geometry (neglecting possible logarithmically weak dependence), Eq. (3) becomes

$$\frac{V_{\mathrm{oc}}}{\rho}=j_L L^2. \tag{11}$$

Here, ρ is the TCO sheet resistance[5] and the right-hand side represents the current generated in the area L^2. Hence, the dead shunt screening length is still given by Eq. (4). Along the same lines one can also extend the results in Eqs. (5)–(7) to the two-dimensional case.

Because of the screening, the electric potential distribution in a dot cell is not uniform. It is sketched in Fig. 4 for a large dot cell $d\gg L$, where d is the cell diameter. The power source contacts the back metal area (dot cell) and the front surface (TCO) at a relatively short distance from the cell edge. The diagram shows the electric potential distributions in the front and back surfaces. The difference between the two represents the local bias distribution in the device. The reasoning behind the diagram is as follows. Far from the metal the local bias equals V_{oc} as there is no current flow

Downloaded 17 Apr 2001 to 209.45.202.202. Redistribution subject to AIP copyright, see http://ojps.aip.org/japo/japcr.jsp

there. It changes drastically towards the metal in a very narrow region, whose dimension (neglected in Fig. 4) is of the order of the screening length $L_s(\ll L_{ds})$ in the bare semiconductor. Typically $L_s \sim (1-100)\ \mu$m as estimated from Eq. (4) where the semiconductor sheet resistance replaces that of the TCO. Because the metal side of the cell is equipotential, we conclude that the electric potential in the back surface changes abruptly at the cell edge and otherwise remains practically constant. We note also that the central inner cell region is screened from the rest of the device $(d \gg L)$, and therefore its local bias equals V_{oc}. Since the local biases in the central region and far from the cell are equal, the corresponding electric potential distributions in these two regions must be parallel, as is shown in Fig. 4. With all of this in mind and taking into account that the resistive potential drop in the front surface balances the total external bias, we arrive at the distributions in Fig. 4. One remarkable feature of it is that only a narrow peripheral region of the cell is active and contributes to its PV properties, while the central region is effectively screened and passive. Hence, the I/V measurements give information only about a limited peripheral part of a large device. This may be especially important for the forward bias measurements where the active area width is exponentially shorter than the cell size.

Note that when the screening is significant, $L \ll d$, the situation effectively reduces to that of the one-dimensional geometry. In particular, the active ring shaped region resistance is of the order of $\rho L/d$. As a result the I/V characteristic analysis in Eqs. (9) and (10) applies to the two-dimensional case with minor changes:

$$I = -\sqrt{\frac{j_L d^2 (V_{oc} - V)}{\rho}} \quad \text{for } V_{oc} - V \ll d^2 j_L \rho, \tag{12}$$

$$I = \sqrt{\frac{(V - V_{oc}) j_L d^2}{\rho}} \exp\left(\frac{q(V - V_{oc})}{2AkT}\right) \quad \text{for } q(V - V_{oc}) \gg kT. \tag{13}$$

Equations (12) and (13) predict that for large cells the measured current density I/d^2 is inversely proportional to the cell diameter, which is verified experimentally further in this article.

III. EXACT RESULTS

Consider a one-dimensional semi-infinite cell in Fig. 1. Putting together Eq. (1) and the Ohm's law in the resistive electrode gives

$$\frac{dJ}{dx} = -j_0\left(\exp\left(\frac{q\varphi}{AkT}\right) - 1\right) + j_L, \qquad J = -\frac{1}{\rho}\frac{d\varphi}{dx}, \tag{14}$$

where J is the current in the resistive electrode and x is the coordinate. The boundary conditions to Eqs. (14) reflect the fact that the perturbation does not affect the electric potential at large distances and that the current through the resistor obeys Ohm's law:

$$\varphi = V_{oc} \quad \text{at} \quad x = \infty, \qquad \frac{\varphi}{R} = J + I \quad \text{at} \quad x = 0. \tag{15}$$

Here, we have introduced the current I generated in the external circuit connected to the resistor in the course of I/V measurements.

Combining Eq. (14) yields a second order differential equation that was noted in Refs. 1–4. Introducing also the dimensionless variables

$$z \equiv \frac{q(V_{oc} - \varphi)}{AkT}, \quad y \equiv \frac{x}{L_0}, \quad L_0 \equiv \sqrt{\frac{AkT}{q\rho(j_0 + j_L)}}, \tag{16}$$

reduces that equation to the form that contains no parameters,

$$\frac{d^2 z}{dy^2} = 1 - \exp(-z). \tag{17}$$

This universal equation was obtained in Ref. 1 in connection with the I/V analysis of the elemental p-n junction. However, it was not fully analyzed and its relation to the electric potential distribution and screening was not recognized at that time. Note that by definition, the characteristic scale L_0 in Eq. (16) represents the length over which the electric potential changes by kT. Lucovsky[6] derived the analogous characteristic length in connection with the problem of lateral photoeffects in nonuniformly irradiated p-n junctions.

While Eq. (17) cannot be solved analytically in the whole range of parameters, it allows approximation that gives accurate analytical results for $z(x)$ separately in the region of $|z| \ll 1$ and in the complementary region. In addition, the I/V characteristic of the system can be derived without explicitly solving Eq. (17). Multiplying Eq. (17) by dz/dy and integrating from zero to finite x gives

$$\frac{1}{2}\left(\frac{dz}{dy}\right)^2 - \frac{1}{2}\left(\frac{dz}{dy}\right)_0^2 = z + \exp(-z) - z(0) - \exp[-z(0)]. \tag{18}$$

Equation (18) is convenient for incorporating the boundary conditions. For the case of large cells we use the boundary conditions in Eq. (15), which in the variables Eq. (16) reduce to

$$-r\frac{dz}{dy} = \frac{q(V_{oc} - IR)}{AkT} - z \quad \text{at} \quad y = 0; \quad r \equiv \frac{R}{\rho L_0}; \qquad z = \frac{dz}{dy} = 0 \quad \text{at} \quad y = \infty. \tag{19a}$$

For the case of small cells of the length l, the second of the above conditions changes to the form

$$\frac{dz}{dy} = 0 \quad \text{at} \quad y = \frac{l}{L_0}, \tag{19b}$$

expressing the absence of current at the cell edge. From this point on, we consider the cases of large and small cells separately.

Downloaded 17 Apr 2001 to 209.45.202.202. Redistribution subject to AIP copyright, see http://ojps.aip.org/japo/japcr.jsp

A. Large cells

1. Electric potential distribution

Substituting into Eq. (18) the boundary conditions Eq. (19a) with $I=0$ gives

$$\frac{1}{2r^2}\left(\frac{qV_{oc}}{AkT}-z(0)\right)^2+1-z(0)-\exp[-z(0)]=0 \tag{20}$$

and

$$\int_{z(0)}^{z}\frac{dz}{\sqrt{z-1+\exp(-z)}}=-\sqrt{2}y. \tag{21}$$

These equations enable one to calculate both the electric potential distribution and its value at the shunt. For convenience, we present results in the standard dimensional variables. For reverse or not very large forward biases, we obtain

$$\varphi\approx V_{oc}-\frac{AkT}{q}\exp\left(-\frac{x}{L_0}\right) \quad \text{for} \quad q(V_{oc}-\varphi)\ll AkT,$$
$$\varphi\approx V_{oc}-(V_{oc}-V_R)\left(1-\frac{x}{L}\right)^2 \quad \text{for} \quad q(V_{oc}-\varphi)\gg AkT, \tag{22}$$

$$L=\sqrt{\frac{2V_{oc}}{(j_0+j_L)\rho}}\sqrt{1-\frac{V_R}{V_{oc}}}. \tag{23}$$

Here, V_R is the voltage across the shunt. If there is no bias applied, then neglecting the last term in Eq. (20) yields

$$\frac{V_R}{V_{oc}}=r'(\sqrt{r'^2+2}-r'),$$
$$r'\equiv r\sqrt{\frac{AkT}{qV_{oc}}}=\frac{R}{\rho L_0}\sqrt{\frac{AkT}{qV_{oc}}}\equiv\frac{R}{R_0}. \tag{24}$$

Note that the screening length L in Eq. (23) differs only by the factor of $\sqrt{2}$ from our simple intuitive estimate in Eq. (5).

For significant forward biases we get

$$\varphi=V_R+\frac{2AkT}{q}\ln\left(1-\frac{x}{L}\right) \quad \text{for} \quad \varphi-V_{oc}\gg AkT/q, \tag{25}$$

$$L=\sqrt{2}L_0\exp\left(-\frac{q(V_R-V_{oc})}{2AkT}\right). \tag{26}$$

Again, the screening length in Eq. (26) is consistent with the result of our qualitative analysis in Eq. (7).

2. I/V characteristics

Substituting Eqs. (19a) into Eq. (18) and putting $R=\infty$ gives

$$I=\pm\frac{\sqrt{2}AkT}{q\rho L_0}\sqrt{\exp\left(-\frac{q(V_{oc}-V)}{AkT}\right)+\frac{q(V_{oc}-V)}{AkT}-1}. \tag{27}$$

The two signs correspond to the cases of $V<V_{oc}(-)$ and $V>V_{oc}(+)$. An example is shown in Fig. 5. The physical meaning of the dependence in Eq. (27) in different regions is explained by our qualitative analysis in Sec. II. The corresponding semiquantitative results in Eqs. (9) and (10) are consistent with Eq. (27).

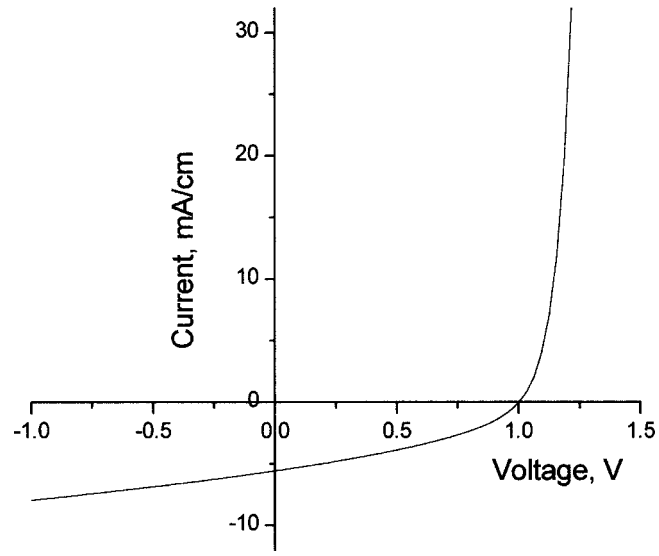

FIG. 5. An example of the I/V characteristic for a large dot cell.

Equation (27) enables one to derive the expressions for the commonly used diode parameters, short-circuit current (I_{sc}) and resistance (R_{sc}), maximum power resistance (R_{mp}), open-circuit resistance (R_{oc}), and the fill factor (FF) (we assume $qV_{oc}\gg AkT$):

$$R_{oc}=L_0\rho, \quad R_{sc}=R_{oc}\sqrt{\frac{2qV_{oc}}{AkT}},$$
$$R_{mp}=R_{oc}\sqrt{\frac{qV_{oc}}{AkT}}, \quad I_{sc}=\frac{\sqrt{2qV_{oc}AkT}}{R_{oc}}, \quad \text{FF}=0.544. \tag{28}$$

The significance of the latter results is that they introduce the regime of large cells where all the characteristics are calculated exactly and which is significantly different from the well-known small cell regime [Eq. (1)].

B. Small cells

To calculate the I/V characteristics we substitute into Eq. (18) the boundary conditions at $y=0$ and $y=l/L$, use the expansions

$$z(l)=z(0)+\frac{l}{L_0}\left(\frac{dz}{dy}\right)_0+\frac{1}{2}\left(\frac{l}{L_0}\right)^2\left(\frac{d^2z}{dy^2}\right)_0,$$

$$\exp[-z(l)]=\exp[-z(0)]-\frac{l}{L_0}\left(\frac{dz}{dy}\right)_0\exp[-z(0)]+\frac{1}{2}\left(\frac{l}{L_0}\right)^2\left(\frac{d^2z}{dy^2}\right)_0\exp[-z(0)],$$

and then express the second derivative from Eq. (17). As a result, we get

Downloaded 17 Apr 2001 to 209.45.202.202. Redistribution subject to AIP copyright, see http://ojps.aip.org/japo/japcr.jsp

$$\left(\frac{dz}{dy}\right)_0 = \frac{l}{L_0}\{\exp[-z(0)]-1\} + \left(\frac{l}{L_0}\right)^2\{\exp[-2z(0)]-1\},$$

which in the standard variables takes the form

$$I = l\left\{j_0\left[\exp\left(\frac{qV}{AkT}\right)-1\right]-j_L\right\} \times\left\{1+\frac{l}{L_0}\left[\exp\left(\frac{q(V-V_{oc})}{AkT}\right)+1\right]\right\}. \tag{29}$$

We note that even for small cells, $l \ll L_0$ the corrections to the standard I/V characteristics become very significant at forward biases ($V > V_{oc}$). In the latter region, the small cell regime has an exponentially narrow domain of applicability $l \ll L_0 \exp(q(V_{oc}-V)/AkT)$. This conclusion is consistent with the discussion in Section II where we have predicted that the characteristic screening length shrinks in the regime of $V > V_{oc}$.

We shall end this section by noting the conclusion that the value of the diode ideality factor A doubles as extracted from the data corresponding to significant forward biases. Indeed, in the region of $V > V_{oc}$ the screening length exponentially shrinks turning the device into the large cell regime, where $I \propto \exp(-qV/kTA_{eff})$ with $A_{eff}=2A$, in accordance with Eqs. (10) and (27). A related prediction is that lowering the illumination intensity may reduce the measured ideality factor by 50%, as the screening length L increase causes the device to operate in the small cell regime.

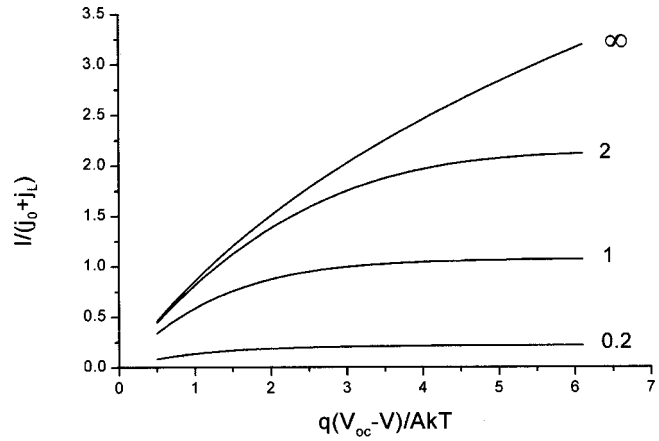

FIG. 6. The dimensionless I/V characteristics of different size linear PV cells in the reverse bias region; $l/L_0 = 0.2,1,2,\infty$.

C. Intermediate size cells

Consider I/V characteristics of finite size PV cells, such that the cell size l is comparable to the screening length, L. We start with the open circuit boundary conditions (19b) at the end of the cell. Multiplying Eq. (17) by dz/dy and integrating from zero to l yields

$$I = \pm\frac{\sqrt{2}AkT}{q\rho L_0}\sqrt{\exp\left(-\frac{q(V_{oc}-V)}{AkT}\right)+\frac{q(V_{oc}-V)}{AkT}-z(l)-\exp(-z(l))}, \tag{30}$$

where $z(l)$ can be determined from

$$\int_{z(0)}^{z(l)}\frac{dz}{\sqrt{z+\exp(-z)-z(l)-\exp[-z(l)]}} = -\sqrt{2}l. \tag{31}$$

The upper (lower) sign in Eq. (30) corresponds to forward (reverse) current direction.

A closed form solution can be obtained for large reverse biases ($z(0) \gg 1$, $z(l) \gg 1$). Equation (31) gives $z(l) = z(0) - l^2/2$, similar to the parabolic potential distribution derived for the semi-infinite strip in Eq. (23). With that, Eq. (30) gives the current $I = -j_L l$, which corresponds to the case of small cells. The physical meaning of the latter result is that a significant reverse bias leads to a large screening length [see Eq. (23)], compared to which the sample size is small.

In the Ohmic region of low biases, $z(0) = q(V_{oc} - V_R)/AkT \ll 1$ (so that $z(l) \ll 1$); and Eqs. (30), (31) can be solved analytically by expanding the exponents in power series,

$$I = \frac{V-V_{oc}}{\rho L_0}\tanh\left(\frac{l}{L_0}\right). \tag{32}$$

In other cases the I/V characteristics can be calculated numerically from Eqs. (30) and (31). Some examples are shown in Fig. 6 (for reverse bias region) and in Fig. 7 (for forward bias region). A cell of the length $l > L$ gradually

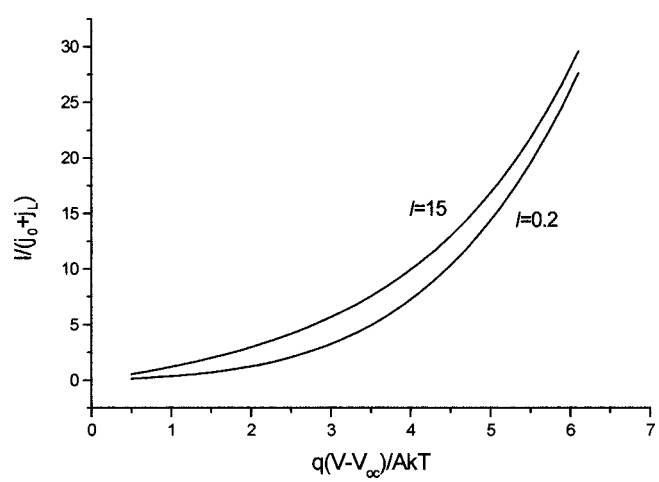

FIG. 7. The dimensionless I/V characteristics of different size linear PV cells in the forward bias region; $l/L_0 = 0.2,15$.

Downloaded 17 Apr 2001 to 209.45.202.202. Redistribution subject to AIP copyright, see http://ojps.aip.org/japo/japcr.jsp

switches from the large cell to the small cell regime with the reverse bias $|V|$. The Ohmic region predicted by Eq. (32) widens in long samples and holds up to $z_0=1.5l$. For the forward bias region, it is seen from Fig. 7 that the I/V characteristic of structure with $l>L$ is always close to that of infinitely long one. This is consistent with the conclusion in the above that the screening length is strongly reduced under forward bias.

One new question related to the finite cell case is that of the boundary condition at the opposite cell end. We consider the case when there is a shunting resistor R_1 at the end of the strip. Then, similarly to Eqs. (19a) and (19b), the boundary conditions at $y=0$ and $y=l$ can be written as

$$-r\frac{dz}{dy}=\frac{q(V_{oc}-IR)}{AkT}-z \quad \text{at} \quad y=0; \quad r\equiv\frac{R}{\rho L_0};$$
$$r_1\frac{dz}{dy}=\frac{qV_{oc}}{AkT}-z \quad \text{at} \quad y=l; \quad r_1\equiv\frac{R_1}{\rho L_0}. \tag{33}$$

The first integral of the Eq. (17) becomes

$$\frac{1}{2}\left(\frac{dz}{dy}\right)^2=z+\exp(-z)-z(l)-\exp[-z(l)]+\frac{1}{2}\left(\frac{dz}{dy}\right)_l^2. \tag{34}$$

This leads to the I/V dependence

$$I=\pm\frac{\sqrt{2}AkT}{q\rho L_0}\sqrt{\exp\left(-\frac{q(V_{oc}-V)}{AkT}\right)+\frac{q(V_{oc}-V)}{AkT}-z(l)-\exp(-z(l))+\frac{1}{2}\left(\left.\frac{dz}{dy}\right|_l\right)^2}. \tag{35}$$

Here the derivative can be expressed from the boundary conditions (33) and the boundary value of the potential $z(l)$ can be found by integration of Eq. (34) over the coordinate.

If the cell is shunted at one end ($x=l$), the open circuit voltage at the other end ($x=0$) depends on the shunt resistance and the cell length l. Some calculations of the voltages at the shunt, $V(l)$ and the open end, $V(0)$ are illustrated in Fig. 8 for a strip of a an intermediate length $l=5L_0$, [close to the screening length in Eq. (4)] as a function of the shunt resistance. The decay of open circuit potential caused by shunting manifests itself when $R_1<\rho l$. At $V(0)$, $V(l)-V_{oc}\gg AkT/q$, and the curves in Fig. 8. are well approximated by the linear dependencies predicted by Eqs. (30) and (31), which in the standard variables take the form

$$V(l)=(j_0+j_L)lR, \quad V(0)=V(l)+\tfrac{1}{2}\rho(j_0+j_L)l^2. \tag{36}$$

They are shown in Fig. 8 by dashed lines.

Let us consider the case of a strong shunt ($R_1\ll\rho L_0$). Then $V(y=l)$ is close to zero ($z(l)=qV_{oc}/AkT$). The results of numerical calculations of the open-end voltage are presented in Fig. 9. The dotted line shows results of approximate dependence for the case when $qV_{oc.}\gg AkT$, i.e., $V(0)=\frac{1}{2}\rho(j_0+j_L)l^2$. Note that the shunt does not manifest itself in I/V characteristics for long strips, $l>[2V_{oc}/(j_0+j_L)\rho]^{1/2}$. The latter equals the screening length in Eqs. (6) and (23) and can be much larger than L_0.

Consider a linear cell with the voltage $V(0)$ at the open end. Applying a biases $V<V(0)$ at that end makes the distribution of the electric potential along the strip nonmonotonic. The quantity $z(\max)$ corresponding to the maximum potential is determined from

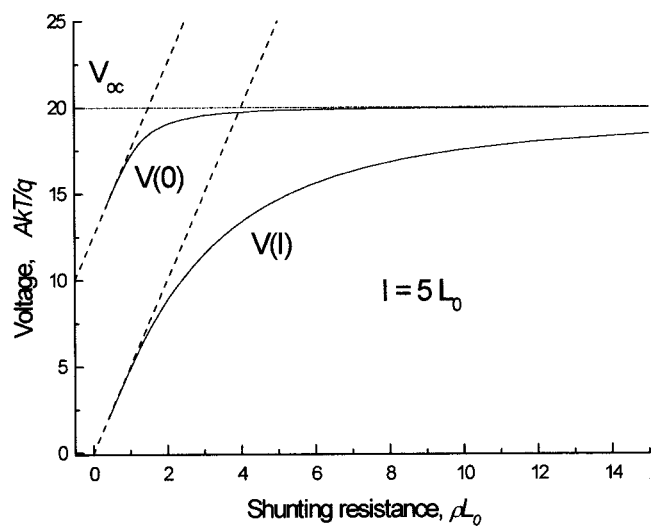

FIG. 8. Open-end, $V(l)$ and shunted-end, $V(0)$ voltages depending on the shunt resistance. Linear approximations in Eq. (36) are shown by dashed lines.

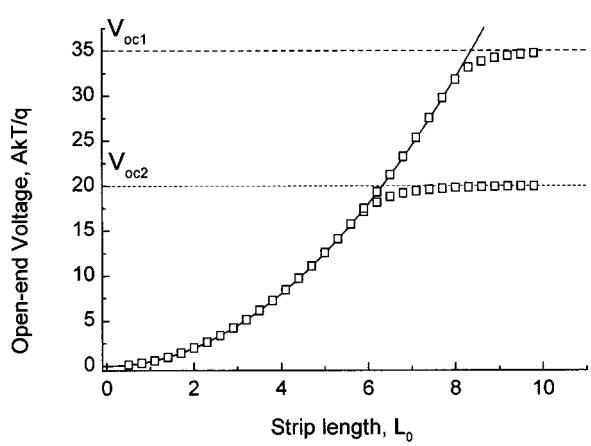

FIG. 9. Open-end voltage in a shunted PV strip vs the strip length calculated for two different V_{oc}. The straight line shows the predicted parabolic dependence.

Downloaded 17 Apr 2001 to 209.45.202.202. Redistribution subject to AIP copyright, see http://ojps.aip.org/japo/japcr.jsp

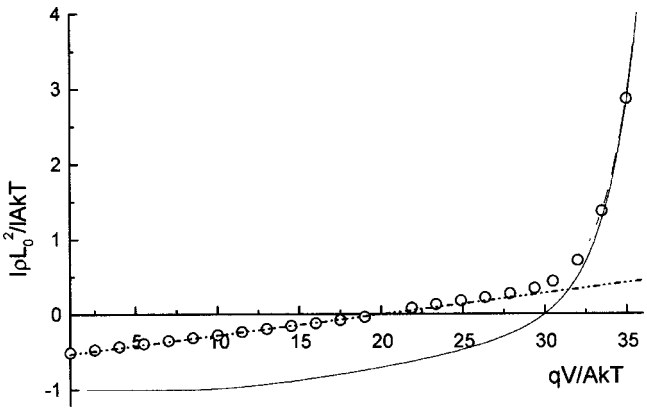

FIG. 10. The calculated I/V characteristic of a shunted cell (open circles) of the length $L=6L_0$ and $V_{oc}/AkT=30$ in comparison with that of unshunted cell (solid curve) and linear fit in Eq. (38).

$$\int_{z(\max)}^{z(l)} \frac{dz}{\sqrt{z+\exp(-z)-z(\max)-\exp[-z(\max)]}} + \int_{z(\max)}^{z(0)} \frac{dz}{\sqrt{z+\exp(-z)-z(\max)-\exp[-z(\max)]}} = -\sqrt{2}l.$$

Given that quantity the reverse current is calculated as

$$I=-\frac{\sqrt{2}AkT}{q\rho L_0}\sqrt{\frac{q(V_{oc}-V)}{AkT}-z(\max)-\exp[-z(\max)]}. \tag{37}$$

This can be further simplified for the region of strong reverse bias, $z(\max)>1$,

$$I=\frac{1}{\rho l}[V-\tfrac{1}{2}(j_0+j_L)\rho l^2]. \tag{38}$$

Equation (38) predicts linear I/V dependence in the region of $I<0$ and is valid for the potentials less than

$$V=-\tfrac{1}{2}\rho(j_0+j_L)l^2. \tag{39}$$

I/V characteristics of a shunted PV strip obtained by numerical calculations is presented in Fig. 10. We note that in the whole range of negative currents, the calculated I/V dependence is very close to that in Eq. (38). To the contrary, in the region of $V>V_{oc}$, the I/V dependence is typical of standard cells and is not sensitive to shunting, reflecting exponentially strong screening in the positive current region.

D. Two-dimensional cells

For the case of a two-dimensional circular cell we replace dJ/dx by div **J** and $d\varphi/dx$ by grad φ in Eq. (14), and introduce the dimensionless variables defined in Eq. (16). We then arrive at Eq. (17) where the Laplacian replaces the second derivative,

$$\nabla^2\varphi=\left(\frac{\partial^2}{\partial y^2}+\frac{1}{y}\frac{\partial}{\partial y}\right)\varphi. \tag{40}$$

If the cell radius is large as compared to the screening length L_0, i.e., $y\gg 1$, the second term in Eq. (40) can be neglected in the proximity of the cell edge. This reduces the equation exactly to the form of Eq. (17), based on which all the subsequent results in Sec. III A can be extended to the two-dimensional case. A minor correction to the I/V characteristic in Eq. (27) is that now the current is obtained as the current density times the cell circumference πd. The latter appears as an additional multiplier in the right-hand side in Eq. (27), consistent with the semiquantitative results in Eqs. (12) and (13). This leads to size dependent I/V characteristics, $I\propto d$. The measured current per area thus becomes inversely proportional to the cell diameter.

For the regime of small two-dimensional cells we proceed from the differential equation $\nabla^2 z=1-\exp(-z)$ and note that any particular function $f(z,y)$ in

$$\frac{1}{y}\frac{\partial z}{\partial y}=f(z,y)$$

leads to

$$\frac{\partial^2 z}{\partial y^2}=f(z,y)+y\frac{\partial}{\partial y}f(z,y).$$

Here the last term is relatively small as $y\ll 1$ and $\partial f/f\partial y\sim 1$, the latter estimate reflecting the fact that $f(z,y)$ does not contain any parameters. Neglecting that term yields

$$2\frac{1}{y}\frac{\partial z}{\partial y}=1-\exp(-z). \tag{41}$$

This can be solved in a closed form to give the electric potential as a function of coordinate (in conventional units)

$$\varphi(x)=V_{oc}-\frac{AkT}{q}\ln\left\{1+\exp\left(\frac{4x^2-d^2}{4L_0^2}\right)\times\left[\exp\left(\frac{q(V_{oc}-V)}{AkT}\right)-1\right]\right\}, \tag{42}$$

where x is the radial distance measured from the center of the cell and V is the electric potential fixed at the cell edge.

To calculate the I/V characteristic we note that $I=-(\pi d/\rho)(\partial\varphi/\partial x)_{x=d/2}$. Expressing the latter derivative from Eq. (41) and adding the neglected term as a first correction gives

$$I=\frac{\pi d^2}{4}\left\{j_0\left[\exp\left(\frac{qV}{AkT}\right)-1\right]-j_L\right\}\times\left[1+\frac{d^2}{4L_0^2}\exp\left(\frac{q(V-V_{oc})}{AkT}\right)\right]. \tag{43}$$

Similar to the one-dimensional result [Eq. (29)], the small cell regime fails at significant forward biases, such that $q(V-V_{oc})\geqslant 2AkT\ln(L_0/2d)$.

We conclude this section by emphasizing two of the above results: (1) we have introduced a new limiting case in the theory of I/V curve analyses (the large cell regime) where all the parameters are calculated exactly and (2) and

Downloaded 17 Apr 2001 to 209.45.202.202. Redistribution subject to AIP copyright, see http://ojps.aip.org/japo/japcr.jsp

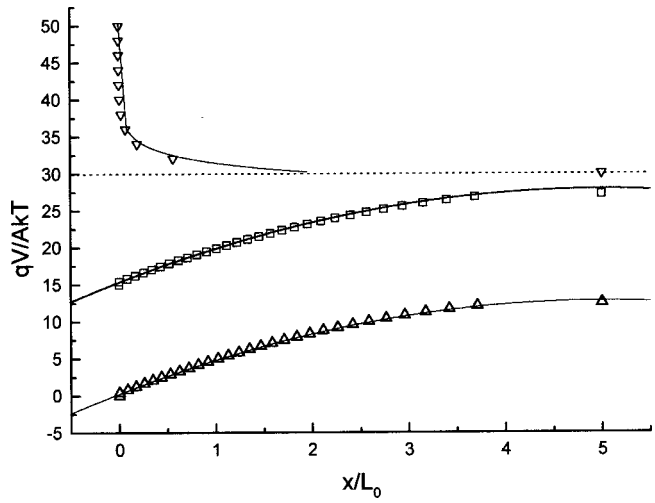

FIG. 11. Numerically simulated distributions of the electric potential (symbols) for forward biased and two reverse biased cells vs analytical fits by Eqs. (23)–(26).

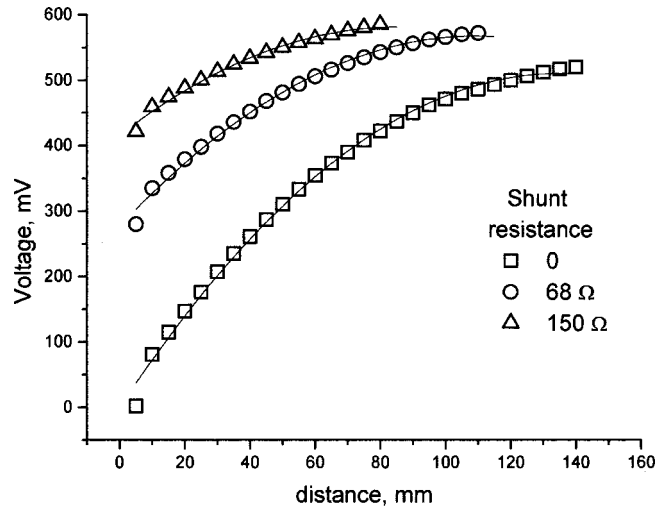

FIG. 13. The measured electric potential distributions in a shunted PV strip for three different shunt resistances in comparison with the analytical fits in Eqs. (23)–(26).

exact results in this section are fully consistent with the much simpler semiquantitative approach developed in Sec. II.

IV. NUMERICAL AND EXPERIMENTAL VERIFICATION

We verified our analytical results in Eqs. (23)–(26) for the electric potential distributions (continuous lines in Fig. 11) by comparing them to the corresponding numerical solutions of Eq. (17) (data points in Fig. 11): good agreement is obtained.

We also used numerical solutions to verify our prediction of size dependent current density [see the discussion after Eqs. (10), (13), (27), and (30)]. One example is shown in Fig. 12 for the case of $V_{oc}/AkT=30$ in one-dimensional model. In all cases, an abrupt transition from the regime of size-independent short-circuit current density to one where the current density is inversely proportional to the cell size occurs at approximately $l=L$.

Direct measurements of the voltage distribution under different biases and light intensities were performed on one-dimensional CdTe/CdS cells using scribe design in Fig. 1. The cell size was 1 cm×20 cm with the TCO sheet resistance of 12 Ω/□. Shown in Fig. 13 are the data corresponding to 1.5% of the standard one-sun light intensity for different shunts. All three dependencies in Fig. 6 are fit by Eq. (23) with $V_{oc}=600$ mV. The best-fit screening radii determined from the fit, 86, 106, and 140 mm relate to each other in accordance with Eq. (23). The measured voltages across the shunts are consistent with Eq. (24) if we put $A=2$.

In Fig. 14, we show the electric potential distributions corresponding to different biases across the cell. We described the reverse bias decay by Eq. (23) where the best fit parameter $L=160$ mm. The ratio of this length to the dead shunt screening length $L=140$ mm is consistent with the theoretically predicted $(V_{oc}/V_{oc}+V)^{1/2}$ [Eq. (23)]. For the case of forward bias, the distributions are fit with Eq. (25),

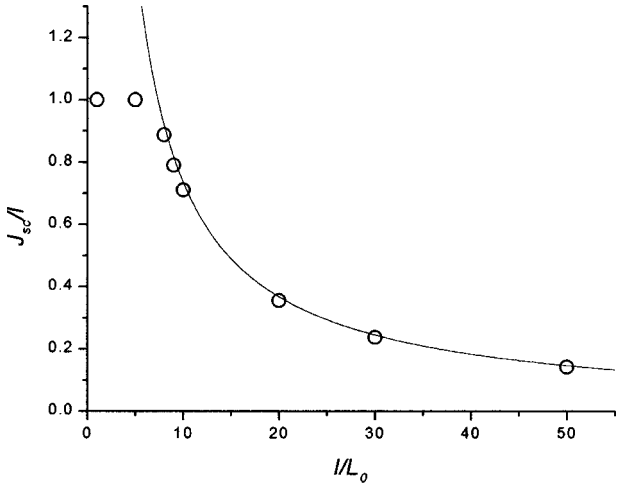

FIG. 12. Specific current in a linear PV strip with $V_{oc}/kT=30$ depending on the strip length. Solid curve represents theoretically predicted dependence $1/l$.

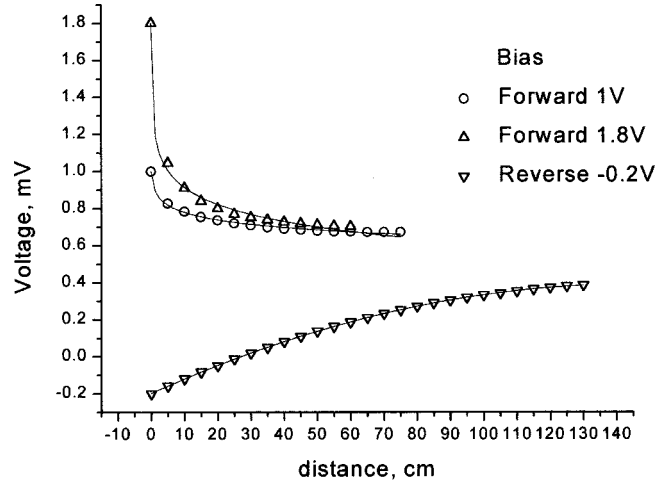

FIG. 14. The measured electric potential distributions for a biased PV strip in comparison with the analytical fits in Eqs. (23)–(25).

Downloaded 17 Apr 2001 to 209.45.202.202. Redistribution subject to AIP copyright, see http://ojps.aip.org/japo/japcr.jsp

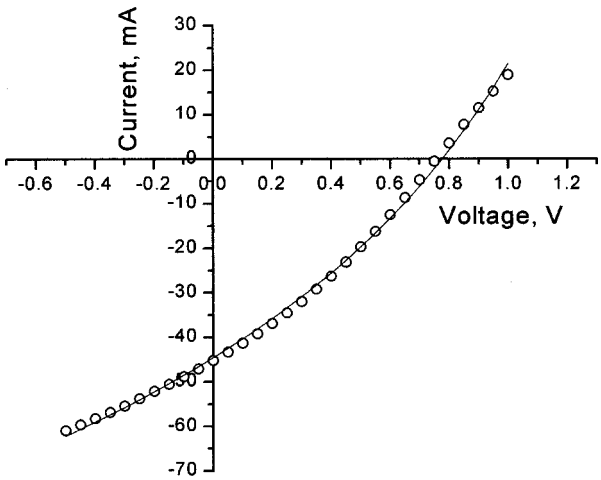

FIG. 15. The measured I/V characteristic of a long linear cell in comparison with the theoretical dependence in Eq. (27).

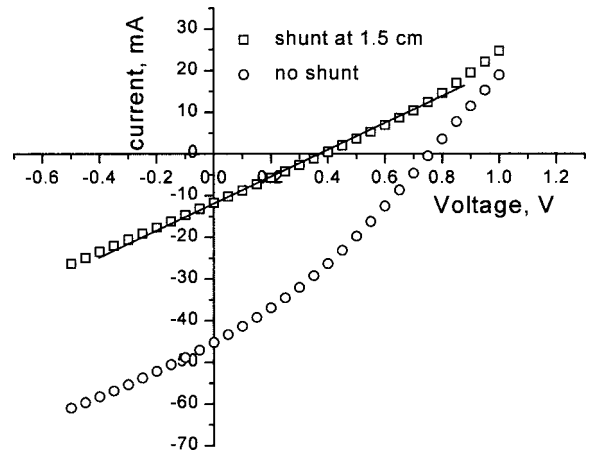

FIG. 17. The measured I/V characteristics of shunted and unshunted cells vs the linear approximation in Eq. (38).

which gives the screening lengths $L=0.014\,\mathrm{mm}$ and $L=0.26\,\mathrm{mm}$ for $V=1.8\,\mathrm{V}$ and $V=1\,\mathrm{V}$, respectively.

Shown in Fig. 15 is the I/V characteristic of a long linear cell in comparison with the theoretical dependence in Eq. (27) that provides a good fit. By measuring I/V characteristics of different length cells we were able to plot the data on J_{sc} versus the cell length as is shown in Fig. 16. These data support the theoretical results in Fig. 12: the l^{-1} dependence is clearly seen for the 1-sun data where the screening length is close to 2.5 cm; for the low light data the screening length of about 15 cm makes the ratio l/L less than 1. In this case, J_{sc} does not depend on l. In Fig. 17, we present the data on I/V characteristics in a shunted cell. In accordance with the prediction in Eq. (38) (and in Fig. 10) the shunted sample I/V characteristic is approximately linear in the negative current region.

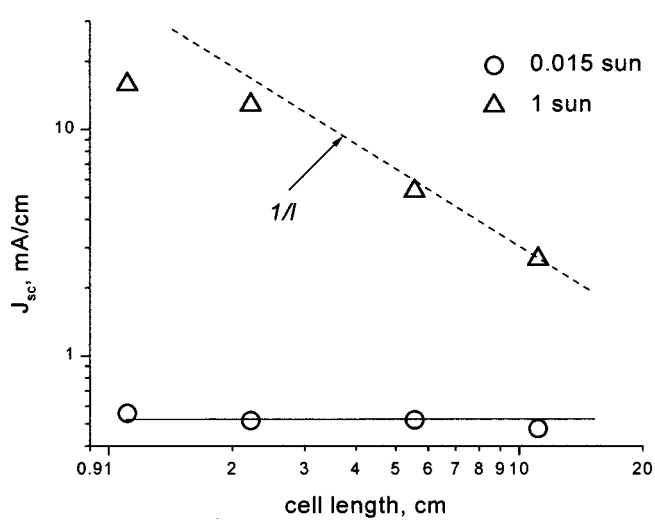

FIG. 16. The measured short circuit current density in a PV strip depending on the strip length for two different illuminations corresponding to the regimes where the strip length is larger or shorter than the screening length.

V. IMPLICATIONS AND CONCLUSIONS

The most straightforward implications of the above results pertain to shunt problems. As an example we note that using Eqs. (23) and (24) enable one to calculate the current loss due to shunts of a given resistance R:

$$J_R=\frac{V_R}{R}$$
$$=\frac{\sqrt{2}V_{oc}}{R}\sqrt{\frac{j_L}{j_c}}\left(\sqrt{\frac{j_L}{j_c}+2}-\sqrt{\frac{j_L}{j_c}}\right),\quad j_c\equiv\frac{V_{oc}\rho}{R^2}.$$

This quantity decays monotonically with R at constant illumination, while as a function of illumination intensity at fixed R it reaches its maximum at $j_L/j_c=0.76$. This can be of interest in connection with the changes in j_L related to different geographical locations and seasons.

Local heating in shunts is often considered a cause for progressive module degradation,[7] and can be expressed from Eq. (23) as

$$P=\frac{V_R^2}{R}=\frac{\sqrt{2}V_{oc}^2}{L_{ds}\rho}r'(\sqrt{r'^2+2}-r')^2.$$

It is a maximum at $r'=0.83$ (corresponding to the shunt resistance $R\sim 20\,\Omega$ for the forementioned device parameters). The nature of the maximum is that a low thermal power generation rate is observed for low R. Similarly, heating is current limited in the case of high R. The above defined extreme shunts are predicted to heat the devices the most. Other potential applications of these results have a bearing upon optimizing cell size in modules (so as to avoid a considerable screening effect and correspondingly considerable fraction of the cell being inactive).

The theory under consideration may be further refined by incorporating effects of back contact resistance that have been neglected. While the results of such a modification will be presented elsewhere, we note here that in some range of the device parameters, taking back contact resistance into account strongly changes these results.

In conclusion, let us summarize the main results of the present consideration. We have introduced a fundamental

Downloaded 17 Apr 2001 to 209.45.202.202. Redistribution subject to AIP copyright, see http://ojps.aip.org/japo/japcr.jsp

concept of screening in PV devices, and have shown that the screening phenomenon is practically important as the characteristic screening length is comparable to the actual cell sizes. In general, the main consequence of screening is that the electric potential distribution across the cell is nonuniform. More specifically, this nonuniformity determines the characteristic area affected by a shunt, and is dependent on the shunt resistance, illumination, and device parameters. The nonuniform potential also determines the relative size of active area in the cell and thus influences the I/V characteristics of the device.

This work was supported in part by NREL Thin-Film Partnership Contract No. ZAK-817619-17. One of the authors (A.V.S.) acknowledges support by the Russian Fund for Basic Research, Project No. 00-02-16775.

[1] B. Ya. Moizhes, Solid State Phys. **2**, 202 (1960).
[2] J. J. Wysocki, RCA Rev. **22**, 57 (1961).
[3] L. D. Nielsen, IEEE Trans. Electron Devices **29**, 821 (1982).
[4] I. L. Eisgruber, J. R. Sites, Proceedings of 24th Photovoltaic Specialists Conference, Hawaii, Dec. 5–9, 1994, p. 271.
[5] For brevity, we use the same letter ρ for specific resistances in both one- and two-dimensional cases, where it has the dimensions of Ω/cm and $\Omega/\square$, respectively
[6] G. Lukovsky, J. Appl. Phys. **31**, 1088 (1960).
[7] M. A. Green, *Solar Cells*, in *Modern Semiconductor Device Physics*, edited by S. M. Sze (Wiley, New York, 1998), p. 473.

Downloaded 17 Apr 2001 to 209.45.202.202. Redistribution subject to AIP copyright, see http://ojps.aip.org/japo/japcr.jsp